Letter

Thermal Control of Engineered T-cells

Mohamad H Abedi, Justin Lee, Dan Ilya Piraner, and Mikhail G. Shapiro

ACS Synth. Biol., **Just Accepted Manuscript** • DOI: 10.1021/acssynbio.0c00238 • Publication Date (Web): 30 Jul 2020

Thermal Control of Engineered T-cells

Mohamad H. Abedi[1], Justin Lee[1], Dan I. Piraner[1], Mikhail G. Shapiro[2,*]

Affiliations:
[1] Division of Biology and Biological Engineering
[2] Division of Chemistry and Chemical Engineering
California Institute of Technology
Pasadena, CA, USA 91125

*Correspondence should be addressed to MGS:
Email: mikhail@caltech.edu
Phone: 626-395-8588 or 617-835-0878
1200 E. California Blvd, MC 210-41, Pasadena, CA 91125

ABSTRACT

Genetically engineered T-cells are being developed to perform a variety of therapeutic functions. However, no robust mechanisms exist to externally control the activity of T-cells at specific locations within the body. Such spatiotemporal control could help mitigate potential off-target toxicity due to incomplete molecular specificity in applications such as T-cell immunotherapy against solid tumors. Temperature is a versatile external control signal that can be delivered to target tissues *in vivo* using techniques such as focused ultrasound and magnetic hyperthermia. Here, we test the ability of heat shock promoters to mediate thermal actuation of genetic circuits in primary human T-cells in the well-tolerated temperature range of 37–42°C, and introduce genetic architectures enabling the tuning of the amplitude and duration of thermal activation. We demonstrate the use of these circuits to control the expression of chimeric antigen receptors and cytokines, and the killing of target tumor cells. This technology provides a critical tool to direct the activity of T-cells after they are deployed inside the body.

Keywords: T-cells, CAR, Thermal Control, Mammalian Synthetic Biology, Heat Shock Promoters, and Immunotherapy.

Unlike small molecule and biologic therapies, cells have a natural ability to navigate, persist and proliferate within the body, providing the potential for more targeted and sustained disease treatment. This potential is enhanced by the capacity of cells to probe, process, and respond to their environment and carry out a wide range of sophisticated behaviors, which can be engineered using the tools of synthetic biology[1]. Among the cell types being developed for therapy, T-cells are one of the most promising due to their central roles in cancer, infectious disease and autoimmune disorders, along with their relative ease of isolation, genetic modification and re-engraftment. For example, this potential has been realized in T-cells engineered to express modularly targeted chimeric antigen receptors (CARs), allowing them to specifically eradicate cancers such as lymphomas bearing the CD19 antigen[2,3,4,5]. Unfortunately, it has been challenging to translate these successful results into solid tumors, where CAR T-cells encounter a more immunosuppressive environment[6] and the risk of sometimes fatal on-target off-tumor toxicity due to the presence of tumor-overexpressed epitopes in healthy tissues[7,8]. Likewise, emerging approaches in which T-cells are used to treat autoimmune disease through local immunosuppression carry the risk of reducing important immune system activity outside the target tissues[9]. Existing strategies seeking to reduce off-target toxicity use additional target recognition elements[10,11] or chemically triggered kill switches[12,13,14]. However, it can be difficult to ensure perfect recognition solely through molecular markers, and premature termination of T-cell therapy using kill-switches turns off their beneficial therapeutic action.

Here we describe a cellular engineering approach to regulate the activity of therapeutic T-cells with greater specificity through a combination of molecular and physical actuation. This approach is designed to take advantage of the ability of technologies such as focused ultrasound (FUS) and magnetic hyperthermia to non-invasively deposit heat at precise locations in deep tissue[15–18]. By engineering thermal bioswitches that allow T-cells to sense small changes in temperature and use them as inputs for the actuation of genetic circuits, we enable these penetrant forms of energy to spatially control T-cell activity. Our approach is based on heat shock promoters (pHSP), which have been shown to drive gene expression in response to FUS-delivered heating[19–21], but have not been tested in primary human T-cells. This is important because the behavior of pHSPs varies greatly between cell types and cellular states. In this study, we screen a library of pHSPs in primary T-cells and engineer gene circuits providing transient and sustained activation of gene expression in T-cells in response to brief thermal stimuli within the well-tolerated temperature range of 37–42ºC[22–24]. Our circuits incorporate feed-forward amplification, positive feedback and recombinase-based state switches. We demonstrate the use of these circuits to control the secretion of a therapeutic cytokine, expression of a CAR, and killing of target tumor cells.

RESULTS

Evaluating candidate pHSPs in primary T-cells. To enable thermal control of T-cell activity, we required a pHSP with robust switching behavior in primary human T-cells. Given the variability in pHSP responses between cell types[25], we decided to systematically evaluate the activity of 13 different pHSPs in response to a 1-hour incubation at 42ºC. This thermal stimulus was chosen based on its tolerability by most tissues[24], and the convenience of relatively short treatment durations in potential clinical scenarios. Our panel of pHSPs included nine human, three mouse, and one C. *elegans* promoters. The human promoters included four naturally occurring sequences (HSPB, HSPB'2, HSP A/A, HSP A/B), two modifications of HSPB'2 generated by varying the 5' UTR (HSPB'1, HSPB'3), and three rational modifications of HSPB'2 (SynHSPB'1, SynHSPB'2, SynHSPB'3) inspired by a previously developed sensor of cellular stress[26]. Truncating HSPB'2 and leaving 192 base pairs resulted in SynHSPB'1. To lower potential baseline activity, the AP-1 binding site in SynHSPB'1 was mutated leading to SynHSPB'2. Duplicating SynHSPB'2 four times to increase the number of heat shock elements (HSE) resulted in SynHSPB'3. The three mouse-derived pHSPs were naturally occurring promoters. HSP16, derived from C. *elegans*, was first described in 1986 and is rationally modified to form a minimal bidirectional promoter encompassing four HSE binding sites[27]. HSP16 excludes other transcription factor binding sites that typically exist in human promoters. We incorporated each pHSP into a standardized lentiviral construct in which the pHSP drives the expression of a green fluorescent protein (GFP), with a constitutively expressed blue fluorescent protein (BFP) serving as a marker of transduction (**Fig. 1a**).

Once stimulated, all of the promoters displayed a uniform level of activation across the cell population allowing us to use mean fluorescence as a metric of fold induction (**Fig. S1**). Of our 13 promoters, HSPB had the lowest baseline expression at 37ºC (**Fig. 1b**), an important property for minimizing activity in the absence of the thermal trigger. HSPB'1 showed the largest fold-change in gene expression, reflecting a combination of relatively low baseline expression and strong promoter activity when stimulated. Among the rationally engineered HSPB'2 variants, SYNHSPB'3 had a lower baseline than the natural promoter, albeit with lower maximum expression on activation. The rest of the human and mouse-derived promoters exhibited high baseline activity, resulting in their elimination from further experiments. Finally, the C. *elegans* minimal promoter exhibited acceptable performance and was included in further testing to investigate whether its minimal composition would be advantageous for specific activation in response to temperature. Based on these factors, we chose HSPB, HSPB'1, SynHSPB'3 and HSP16 as our starting points for further circuit engineering.

Thermal parameters for pHSP activation. After identifying four candidate pHSPs, we tested their response to a range of induction parameters. To search for temperatures that provide rapid induction with minimal

thermal burden to the cells, we incubated pHSP-transduced T-cells at temperatures ranging from 37°C to 44°C for 1 hour. All four promoters exhibited a significant increase in activity starting at 42°C (**Fig. 2a**). Increasing the induction temperature beyond this point resulted in a significant enhancement of transcriptional activity, but compromised cell viability (**Fig. 2b**). To optimize induction with minimal cell damage, we chose 42°C for further experiments. We note that unlike the gradual increase in gene expression observed with the mammalian promoters above 42°C, HSP16 exhibited a large jump between this temperature and 43°C, which may make it useful in future circuit engineering applications.

To reduce the effect of thermal exposure on cell viability, we tested a pulsatile heating scheme with a 50% duty cycle[28]. In this scheme, cells underwent repeated cycles of heating to 42°C for a fixed duration and an equal amount of time at 37°C, adding up to a total of one hour at 42°C over a two-hour treatment period. We varied the stimulation period between one minute and continuous heating for 60 min. This experiment revealed a trade-off between promoter activity (**Fig. 2c**) and cell viability (**Fig. 2d**), with shorter pulses reducing the former while increasing the latter. For the purposes of T-cell therapy, in which cells can expand after activation, we decided that a 40% decrease in cell viability was a suitable trade-off for improved activation, therefore selecting a continuous heating paradigm. This paradigm also simplifies the application of heating during therapy. We also investigated continuous stimulation durations ranging from 15 to 120 minutes. Shorter induction enhanced viability (**Fig. 2e**) at the expense of lower gene expression (**Fig. 2f**), with a one-hour stimulation providing a reasonable balance. While the optimal stimulation scheme would heavily depend on the promoter used, circuit design, targeted tissue, and therapeutic dose required, we chose a one-hour continuous stimulus at 42°C as our heating paradigm for our subsequent experiments to maximize our chances of getting a meaningful response despite some damage to the cells.

Genetic circuits for amplified and sustained thermal activation. On their own, pHSPs drove a relatively small amount of transient protein expression upon induction. To enable the use of pHSPs in T-cell therapy applications, it is useful to amplify the output of pHSP-driven circuits. This would enable cells to, for example, release a relatively large therapeutic bolus after a single thermal stimulus. To achieve this goal, we implemented a feed-forward amplification circuit in which the pHSP drives an rtTA transactivator, which produces stronger transcriptional activation tunable with doxycycline. In addition, LNGFR was constitutively expressed to identify virally transfected cells (**Fig. 3a**). Amplification circuits incorporating HSPB, HSPB'1, SynHSPB'3 and HSP16 all exhibited a substantial increase in their fold-induction, while only modestly elevating baseline expression. HSPB showed the best performance, suggesting that in the context of feed-forward amplification driving the maximum expression level, a promoter with lower leakage (**Fig. 1b**) is preferable. The expression of a constitutive transduction marker was similar across constructs (e.g. **Fig. S2**), indicating that infection levels did not affect their relative performance. To further tune the

performance of the HSPB amplifier circuit, we designed constructs with reduced translation of the GFP by varying the Kozak sequence or inserting a micro open reading frame upstream[29] (**Fig. 3b**). These modifications enabled the tuning of both the baseline expression and the maximal activation level.

In some therapeutic scenarios, it is critical to prolong the therapeutic action of T-cells following a thermal induction treatment. This would eliminate the need to apply repeated stimuli to maintain treatment efficacy. To develop this capability, we established a positive feedback amplifier circuit by rearranging the elements of our feed-forward amplifier such that rtTA could drive its own expression in the presence of doxycycline (**Fig. 3c**). A similar design was previously tested in human cervical cancer HeLa cells[30]. The HSPB feedback circuit maintained its thermal induction level, and we were able to reduce baseline activity by tuning the Kozak sequence upstream of rtTA. In the current design, the output of the positive feedback circuit is lower than that of the feed-forward amplifier, as expected from the GFP payload being placed after an IRES element. While we envision that such "low but steady" activity is desirable in many applications, a "high and steady" mode could in principle be achieved by exchanging the IRES for a 2A element. The dynamic expression profiles of our direct, feed-forward, and feedback HSPB circuits are compared in **Fig. 3d**, demonstrating prolonged expression with positive feedback.

While the positive feedback circuit sustained expression for several days, this circuit can eventually turn off amid dilution or fluctuating expression of the transactivator. To establish a permanent thermal switch, we tested gene circuits in which we placed the expression of CRE recombinase under the control of candidate pHSPs (**Fig. 3e**). In these circuits, the pHSP-driven expression of CRE permanently toggles the circuit from expressing RFP to expressing anti-CD19 CAR by recombining the target vector. When tested in a Jurkat T-cell line, these circuits demonstrated robust activation and minimal leakage (**Fig. 3f**). However, when tested in primary T-cells, we observed significantly higher levels of background activation (**Fig. 3f**). This may arise from the fact that immune stimulation is used to maintain primary T-cells in culture and our finding, discussed below, that pHSPs show significant background activity in stimulated primary T-cells. Taken together, these results suggest that in primary T-cells, feed-forward and feed-back amplification provide robust methods for thermal control of gene expression, while pHSP-controlled CRE recombination may produce an unacceptable level of irreversibly accumulating background activation.

Temperature-activated cytokine release. To demonstrate the ability of our positive feedback circuit to sustain a therapeutically relevant function after thermal induction, we connected its output to the production of a cytokine. The local delivery of cytokines from engineered T-cells would be useful in cancer immunotherapy by allowing T-cells to secrete immune-stimulatory factors to remodel the tumor microenvironment and reduce immunosuppression. It would also be useful in treatments of autoimmune disease by allowing T-cells to secrete factors locally down-regulating the activity of endogenous immune

cells. As a model cytokine, we selected IL-21, which has potential utility in cancer immunotherapy due to its ability to stimulate NK cells and $CD8^+$ T-cells[31,32]. We incorporated human IL-21 in place of GFP in our positive feedback circuit (**Fig. 4a**). Without thermal induction, primary T-cells transduced with this circuit produced minimal IL-21. Once stimulated, the cells rapidly secreted IL-21, reaching a near-maximal level by 12 hours, and sustained activity for at least 5 days (**Fig. 4a**). The dependence of continued circuit function on doxycycline provides an additional layer of control, allowing the termination of therapy production at a desired time by removing doxycycline. To demonstrate this capability, we removed doxycycline 24 hours after cell induction, resulting in the abrogation of cytokine production by day five. The ability to chemically terminate the activity of our circuit enhances its safety profile in potential therapeutic applications.

In some scenarios, it would be useful for cytokine release to be triggered from a T-cell constitutively expressing a CAR, allowing the cytokine to locally boost immune activation during CAR-directed killing. To test this possibility, we co-transduced primary T-cells with our positive IL-21 circuit and a constitutively expressed anti-CD19 CAR (**Fig. 4b**). In the absence of target Raji bait cells expressing CD19, IL-21 release was well-controlled by thermal induction (**Fig. 4b**). However, co-incubation with bait cells resulted in the activation of IL-21 release after 3 days in co-culture even in the absence of a thermal treatment (**Fig. 4b**). These results suggested that HSP activity may be driven by T-cell stimulation, as evidenced by IL-21 release. However, since certain subsets of T-cells have been shown to release endogenous IL-21 when stimulated[33], we set out to directly test the induction of pHSP upon T-cell stimulation using a non-cytokine output, as discussed below.

Dependence of pHSP-driven circuits on T-cell activation. To directly examine the possibility that pHSPs are turned on in response to CAR-driven T-cell activation, we tested the expression of pHSP-driven GFP in constitutively CAR-expressing T-cells (**Fig. 5a**) upon exposure to a thermal stimulus or bait cells. We found that both thermal stimulation and CAR engagement lead to pHSP-driven gene expression (**Fig. 5b**). This response occurred in cells expressing circuits based on HSPB, SynHSPB'3 and HSPmin promoters. Because SynHSPB'3 lacks the AP-1 site present in wild-type pHSPs such as HSPB, and HSPmin is composed of only HSE binding sites driving a minimal promoter, these results suggest that pHSP induction takes place via an HSF1-mediated mechanism. This unexpected finding suggests that activated T-cells experience cellular stress – for example due to rapid proliferation – potentially resulting in an increased number of mis-folded proteins, leading to HSP upregulation. This provides an important insight for the design of thermally inducible immunotherapies.

Auto-sustained thermally induced CAR expression and tumor cell killing. Our finding that CAR engagement drives pHSP activity suggested that a simple, auto-sustained gene circuit could drive CAR-mediated killing in response to the combination of a thermal stimulus and the presence of target cells. In particular, we hypothesized that placing CAR expression under the control of a pHSP (**Fig. 6a**) would result in T-cells with no initial CAR expression or activity, even in the presence of target cells. Upon thermal induction, CAR would become transiently expressed. If the CAR target is present in the vicinity of T-cells, these cells would become activated, driving sustained expression of additional CAR from the pHSP and target cell killing.

As predicted, this pHSP-CAR circuit showed no baseline CAR expression in primary T-cells, but began to express CAR when thermally stimulated (**Fig. 6a**). CAR expression was greatly reduced after 24 hours in the absence of target engagement (**Fig. 6b**). When cultured with $CD19^+$ bait cells (**Fig. 6c**), thermally activated pHSP-CAR T-cells eliminated the bait cells after 9 days in co-culture (**Fig. 6d, Fig. S3**). This killing was as complete as with positive control T-cells carrying a constitutively expressed CAR driven by the EF1α promoter, albeit over a longer time span. This difference may be due to the maximum level of pHSP-driven CAR expression being lower than the level observed with a constitutive EF1α promoter (**Fig. S4**). When pHSP-CAR T-cells and bait cells were co-incubated without thermal stimulation, no apparent killing took place. While the initial thermal stimulus results in some cell death, T-cells maintain their proliferative capacity and rapidly make up for the initial loss in T-cells (**Fig. S5**). These results suggest that a thermal stimulus can kick-start a positive feedback loop of activation-driven expression of CAR from pHSP, leading to effective bait cell elimination. This activation paradigm could help with mitigating off-target toxicity since CAR expression will be abrogated once T-cells leave the tumor site.

DISCUSSION

Our results demonstrate that engineered bioswitch circuits using pHSP can provide control of T-cell therapy with mild hyperthermia. While it has been previously shown that light-switchable proteins could also confer spatiotemporal control over T-cell activity[34], light has poor penetration into tissues, limiting the utility of such tools. On the other hand, temperature can be elevated at arbitrary depth and with high spatial precision using non-invasive methods such as FUS or magnetic hyperthermia[15–18].

Our study showed that temperatures in the well-tolerated range of 37-42ºC[35,36] can provide control over T-cell function, including the synthesis and release of a cytokine and the CAR-mediated killing of cancer cells *in vitro*, with minimal baseline activity. In future studies, this performance must be characterized and optimized in the *in vivo* setting. In particular, it will be useful to optimize the thermal

requirements of ultrasound activation. While thermal tissue damage is not a major concern in tumor therapy (where it can be synergistic), damage to healthy tissues in non-tumor applications could be detrimental[35,36]. It would also be desirable to shorten the FUS treatment duration to substantially less than the 1 hour heat pulse used in this study. Further promoter engineering, protein engineering and thermal pulse optimization could broaden the range of applications for this technology.

Despite their name, pHSPs can respond to a variety of stimuli such as heat, hypoxia, heavy metals, cytokines and cell division[37,38]. Therefore, the context in which these promoters are being used must be carefully considered. In this work, we capitalized on non-thermal pHSP induction by the T-cell receptor pathway to generate sustained killing circuits. In other contexts where the promiscuous responsiveness of pHSPs presents an un-exploitable hindrance, it may be desirable to develop thermal response mechanisms based on orthogonal molecular bioswitches[22,23].

METHODS

Plasmid Construction and Molecular Biology

All plasmids were designed using SnapGene (GSL Biotech) and assembled via reagents from New England Biolabs for KLD mutagenesis (E0554S) or Gibson Assembly (E2621L). After assembly, constructs were transformed into NEB Turbo (C2984I) and NEB Stable (C3040I) *E. coli* for growth and plasmid preparation. The CAR-CD19 gene containing the CD28 and CD3z signaling domain was a kind gift from the Laboratory of David Baltimore (Caltech). Integrated DNA Technologies synthesized other genes, the pHSP, and all PCR primers. Kozak used in figure 3B: CGG-ATG for 75% and ACCATGGGTTGAGCC-ATG for 10%. The original kozak was ACC-ATG.

Cell Lines

Raji cells (CCL-86) were obtained from ATCC and cultured in RPMI 1640 media (Thermo Fisher Scientific) with 1x Penicillin/Streptomycin (Corning). 1000 ng/ml of doxycycline was used for induction of the Tet promoter. GFP^+ Raji cells were constructed via viral infection of a GFP driven by the EF1a promoter. Lentivirus was prepared using a third-generation viral vector and helper plasmids (gifts of D. Baltimore). Virus was packaged in HEK293T cells grown in 10 cm dishes. After 3 days of transfection, viral particles were concentrated via Ultracentrifugation. Infection was performed by following the "RetroNectin" (T100B Takara Bio) reagent protocol. Experiments were performed at least two weeks after infection.

Primary T-cells

T-cells were isolated with the EasySep Human T-cell isolation Kit (STEMCELL Technologies 17951) from frozen human peripheral blood mononuclear cells obtained from healthy donors. T-cells were stimulated with CD3/CD28 Dynabeads (Thermo Fisher Scientific 11132D) at 1:1 cell:bead ratio for 1 day before viral transduction. Dynabeads were removed on day seven and the cells were allowed to rest until day fourteen before proceeding with experiments. This delay was designed to avoid any activation interference with HSP activity. T-cells were cultured in RPMI supplemented with 50 U/ml IL-2 (Miltenyi Biotech 130-097-744) and 1 ng/ml IL-15 (Miltenyi Biotech 130-095-762) every other day. T-cells were enriched by LNGFR magnetic bead based sorting (Miltenyi Biotech 130-091-330) when appropriate.

Thermal Regulation Assay

Thermal stimulation of T-cells was performed in a Bio-Rad C1000 thermocycler. T-cells at 1-2 million/ml were supplemented with doxycycline, if needed, and mixed well before transferring 50 µl into a sterile PCR tube. The temperature and duration of stimulation was varied based on the experimental procedure. Upon completion of thermal stimulation, cells were moved back into a mammalian incubator and supplemented

1:1 with fresh media containing cytokines and in some cases doxycycline. Cells were typically incubated for 24 hours unless stated otherwise before assaying with a flow cytometer (MACSQuant VYB). Dead cells were typically excluded via FSC/SSC gating for routine assays. In Figure 2, a LIVE/DEAD viability/cytotoxicity kit (Thermo Fisher L3224) was used for a more accurate quantification of cell state. Live cells were further gated via a transfection marker to isolate virally infected cells for further analysis. The change in mean fluorescence of the cell population was used to characterize the fold change of pHSP constructs. To account for cellular auto-fluorescence, the mean fluorescence signal from non-transduced T-cells was collected in each experiment and subtracted from the mean fluorescence of experimental T-cells. Anti-HA antibodies (Miltenyi Biotech 130-120-722) were used to stain for CAR expression and V450 Mouse Anti-human CD271 was used to stain LNGFR (BD biosciences 562123). IL-21 expression was measured using a human IL-21 DuoSet ELISA (R&D systems DY8879-05).

T-cell Bait Assay

Raji and GFP^+ Raji cells were used as bait cells for CAR-CD19 T-cells. Bait assays were initiated by mixing T-cells with bait cells at a 3:1 ratio. This ratio was established to avoid excessive bait cell growth before T-cell engagement. To assess T-cell killing of bait cells GFP^+ Raji were used and the count of GFP^+ cells was tracked over time.

Data and code availability

Plasmids will be made available through Addgene upon publication. All other materials and data are available from the corresponding author upon reasonable request.

AUTHOR INFORMATION

Corresponding author: mikhail@caltech.edu.

The authors declare no competing financial interests.

AUTHOR CONTRIBUTIONS

M.H.A. and M.G.S. conceived the study. M.H.A., J.L. and D.I.P. planned and performed experiments. M.H.A. and J.L. analyzed data. M.H.A. and M.G.S. wrote the manuscript with input from all other authors. M.G.S. supervised the research.

ACKNOWLEDGEMENTS

The authors thank Ellen Rothenberg, David Baltimore, Arnab Mukherjee, and Yvonne Chen for helpful discussions. The authors thank Siavash Ahrar and Shirin Shivaei for helpful input on the manuscript.

FUNDING SOURCES

This research was supported by the Sontag Foundation (to M.G.S.) and the Defense Advanced Research Project Agency (D14AP00050 to M.G.S.). M.H.A. was supported by the NSF graduate research fellowship and the Paul and Daisy Soros Fellowship for New Americans. J.L. was supported by the Paul and Daisy Soros Fellowship for New Americans. Related research in the Shapiro laboratory is supported by the Burroughs Welcome Career Award at the Scientific Interface, the Packard Fellowship in Science and Engineering and the Heritage Medical Research Institute.

Supplementary Material

Supplementary Figures S1-6; This includes (i) Thermally induced shift in gene expression, (ii) Expression of a transduction marker to control for variability in infection, (iii) Bait cell count for the HSP CAR killing experiment, (iv) CAR expression from constitutive and induced constructs, (v) Assessing the proliferative capacity of stimulated T-cells, (vi) Assessing thermally induced CAR expression levels.

FIGURE LEGENDS

Figure 1 | Evaluating candidate pHSPs in primary T-cells (a) Illustration of the screening strategy used to characterize the behaviour of pHSPs. The viral construct used to assay pHSPs is shown, along with the promoters tested. LTR, long terminal repeat. (b) Mean fluorescence intensity 24 hours after a 1-hour incubation at 37°C or 42ºC, as measured via flow cytometry. The fold change between 37°C and 42°C is listed above each sample. Where not seen, error bars (±SEM) are smaller than the symbol. N=3 biological replicates for each sample.

Figure 2 | Thermal parameters for pHSP activation in primary human T-cells. GFP expression from constructs driven by the HSPB, HSPB'1, SynHSPB'3 and HSP16F promoters (a, c, e) and T-cell viability (b, d, f) as a function of (a,b) induction temperature for a continuous 1 hour stimulus, (c,d) pulse duration of stimuli delivered with a 50% duty cycle alternating between 37ºC and 42ºC for a fixed thermal exposure of 1 hour, and (e,f) induction duration for continuous heating at 42ºC. Where not seen, error bars (±SEM) are smaller than the symbol. N=3 biological replicates for each sample.

Figure 3 | Genetic circuits for amplified and sustained thermal activation. (a) Diagram illustrating the thermally trigged feed-forward circuit (top). Fluorescence analysed 24 hours post a 1-hour induction at 37º or 42ºC for cells supplemented with doxycycline (bottom). (b) Diagram illustrating a feed-forward circuit driven by HSPB, <K> indicates varying kozak strength (top). Fluorescence analysed 24 hours post a 1-hour induction at 37º or 42ºC for cells supplemented with doxycycline (bottom). The HSPB data is the same as in panel (a), and is re-shown here to facilitate comparisons. (c) Diagram illustrating the thermally trigged positive feedback circuit (top). Fluorescence analysed 24 hours post a 1-hour induction at 37º or 42ºC for cells supplemented with doxycycline (bottom). (d) Normalized expression monitored over seven days after a 1-hour induction at 42ºC for direct HSPB-driven, feed-forward HSPB and positive-feedback HSPB circuits. Circuits have been modified to replace GFP with a destabilised version of the protein. (e) Illustration of the CRE based thermally triggered permanently stable switch designed to express CAR-CD19 upon induction. (f) Cells were either incubated at 37ºC or thermally stimulated for 1 hour at 42ºC and analysed 24 hours later to determine the number of activated cells. Where not seen, error bars (±SEM) are smaller than the symbol. N=3 biological replicates for each sample.

Figure 4 | Temperature activated cytokine release. (a) Diagram illustrating the positive feedback circuit used to express IL-21 (top). Cumulative IL-21 release from 1-hour induction at 37º or 42ºC. In one sample, doxycycline was removed after 24 hours (bottom). (b) Illustration of the constructs used to assay the ability of CAR activity to trigger expression of IL-21 in the feedback pHSP circuit (top). Cells were either incubated at 37C or thermally stimulated for 1 hour at 42ºC with and without bait cells (bottom). Media was collected and frozen at each time point and all samples were analysed simultaneously at the end of collection. Cumulative IL-21 expression was quantified by using an IL-21 ELISA. Where not seen, error bars (±SEM) are smaller than the symbol. N=3 biological replicates for each sample.

Figure 5 | Dependence of pHSP-driven circuits on T-cell activation. (a) Illustration of the constructs used to assay the ability of CAR activity to trigger pHSP. (b) Cells were either incubated at 37ºC, thermally stimulated for 1 hour at 42ºC, or incubated with $CD19^+$ bait cells. pHSP triggered activity was determined by quantifying GFP expression 24 hours after induction. Where not seen, error bars (±SEM) are smaller than the symbol. N=3 biological replicates for each sample.

Figure 6 | Auto-sustained thermally induced CAR expression and tumor cell killing. (a) Illustration of the viral construct used to assay pHSP (SynHSPB'3)-driven expression of CAR-CD19. Cells were either incubated at 37ºC or thermally stimulated for 1 hour at 42ºC and pHSP-triggered CAR-CD19 expression was quantified by surface staining of an HA tag appended to the CAR 12 hours after induction. N=3 biological replicates. (b) CAR-CD19 expression 6, 12, and 24 hours after 1-hour induction with 37ºC or

42ºC. N=3 biological replicates. Negative values in 37°C samples result from subtraction of signal acquired from wild-type T-cells. Raw data is provided in **(Fig. S6)**. **(c)** Illustration of the viral construct and assay used to test the ability of pHSP-inducible CAR expression to conditionally kill bait cells. Cells were either incubated at 37°C or thermally stimulated for 1 hour at 42ºC before being incubated with $CD19^+$ bait cells. **(d)** Unmodified T-cells and T-cells constitutively expressing CAR-CD19 were used as a negative and positive control respectively. pHSP (SynHSPB'3) triggered killing activity was quantified by counting the % of bait cells alive compared to the negative control for a duration of 13 days. N= 3 biological replicates for two T-cell collections from different patients, total N=6. Where not seen, error bars (±SEM) are smaller than the symbol.

REFERENCES

(1) P Teixeira, A., and Fussenegger, M. (2019) Engineering mammalian cells for disease diagnosis and treatment. *Curr. Opin. Biotechnol. 55*, 87–94.
(2) Brentjens, R. J., Davila, M. L., Riviere, I., Park, J., Wang, X., Cowell, L. G., Bartido, S., Stefanski, J., Taylor, C., Olszewska, M., Borquez-Ojeda, O., Qu, J., Wasielewska, T., He, Q., Bernal, Y., Rijo, I. V., Hedvat, C., Kobos, R., Curran, K., Steinherz, P., Jurcic, J., Rosenblat, T., Maslak, P., Frattini, M., and Sadelain, M. (2013) CD19-Targeted T Cells Rapidly Induce Molecular Remissions in Adults with Chemotherapy-Refractory Acute Lymphoblastic Leukemia. *Sci. Transl. Med. 5*, 177ra38-177ra38.
(3) Turtle, C. J., Hanafi, L.-A., Berger, C., Gooley, T. A., Cherian, S., Hudecek, M., Sommermeyer, D., Melville, K., Pender, B., Budiarto, T. M., Robinson, E., Steevens, N. N., Chaney, C., Soma, L., Chen, X., Yeung, C., Wood, B., Li, D., Cao, J., Heimfeld, S., Jensen, M. C., Riddell, S. R., and Maloney, D. G. (2016) CD19 CAR-T cells of defined CD4+:CD8+ composition in adult B cell ALL patients. *J. Clin. Invest. 126*, 2123–2138.
(4) Brentjens, R. J., Rivière, I., Park, J. H., Davila, M. L., Wang, X., Stefanski, J., Taylor, C., Yeh, R., Bartido, S., Borquez-Ojeda, O., Olszewska, M., Bernal, Y., Pegram, H., Przybylowski, M., Hollyman, D., Usachenko, Y., Pirraglia, D., Hosey, J., Santos, E., Halton, E., Maslak, P., Scheinberg, D., Jurcic, J., Heaney, M., Heller, G., Frattini, M., and Sadelain, M. (2011) Safety and persistence of adoptively transferred autologous CD19-targeted T cells in patients with relapsed or chemotherapy refractory B-cell leukemias. *Blood 118*, 4817–4828.
(5) Kochenderfer, J. N., Wilson, W. H., Janik, J. E., Dudley, M. E., Stetler-Stevenson, M., Feldman, S. A., Maric, I., Raffeld, M., Nathan, D.-A. N., Lanier, B. J., Morgan, R. A., and Rosenberg, S. A. (2010) Eradication of B-lineage cells and regression of lymphoma in a patient treated with autologous T cells genetically engineered to recognize CD19. *Blood 116*, 4099–4102.
(6) Zhang, Y., and Ertl, H. C. J. (2016) Starved and Asphyxiated: How Can CD8(+) T Cells within a Tumor Microenvironment Prevent Tumor Progression. *Front. Immunol. 7*, 32.
(7) Morgan, R. A., Chinnasamy, N., Abate-Daga, D., Gros, A., Robbins, P. F., Zheng, Z., Dudley, M. E., Feldman, S. A., Yang, J. C., Sherry, R. M., Phan, G. Q., Hughes, M. S., Kammula, U. S., Miller, A. D., Hessman, C. J., Stewart, A. A., Restifo, N. P., Quezado, M. M., Alimchandani, M., Rosenberg, A. Z., Nath, A., Wang, T., Bielekova, B., Wuest, S. C., Akula, N., McMahon, F. J., Wilde, S., Mosetter, B., Schendel, D. J., Laurencot, C. M., and Rosenberg, S. A. (2013) Cancer regression and neurological toxicity following anti-MAGE-A3 TCR gene therapy. *J. Immunother. 36*, 133–151.
(8) Morgan, R. A., Yang, J. C., Kitano, M., Dudley, M. E., Laurencot, C. M., and Rosenberg, S. A. (2010) Case Report of a Serious Adverse Event Following the Administration of T Cells Transduced With a Chimeric Antigen Receptor Recognizing ERBB2. *Mol. Ther. 18*, 843–851.
(9) Ellebrecht, C. T., Bhoj, V. G., Nace, A., Choi, E. J., Mao, X., Cho, M. J., Zenzo, G. D., Lanzavecchia, A., Seykora, J. T., Cotsarelis, G., Milone, M. C., and Payne, A. S. (2016) Reengineering chimeric antigen receptor T cells for targeted therapy of autoimmune disease. *Science 353*, 179–184.
(10) Zah, E., Lin, M.-Y., Silva-Benedict, A., Jensen, M. C., and Chen, Y. Y. (2016) T Cells Expressing CD19/CD20 Bispecific Chimeric Antigen Receptors Prevent Antigen Escape by Malignant B Cells. *Cancer Immunol. Res. 4*, 498–508.
(11) Roybal, K. T., Rupp, L. J., Morsut, L., Walker, W. J., McNally, K. A., Park, J. S., and Lim, W. A. (2016) Precision Tumor Recognition by T Cells With Combinatorial Antigen-Sensing Circuits. *Cell 164*, 770–779.
(12) Traversari, C., Marktel, S., Magnani, Z., Mangia, P., Russo, V., Ciceri, F., Bonini, C., and Bordignon, C. (2007) The potential immunogenicity of the TK suicide gene does not prevent full clinical benefit associated with the use of TK-transduced donor lymphocytes in HSCT for hematologic malignancies. *Blood 109*, 4708–4715.
(13) Di Stasi, A., Tey, S.-K., Dotti, G., Fujita, Y., Kennedy-Nasser, A., Martinez, C., Straathof, K., Liu, E., Durett, A. G., Grilley, B., Liu, H., Cruz, C. R., Savoldo, B., Gee, A. P., Schindler, J., Krance, R. A., Heslop, H. E., Spencer, D. M., Rooney, C. M., and Brenner, M. K. (2011) Inducible apoptosis as a safety switch for adoptive cell therapy. *N. Engl. J. Med. 365*, 1673–1683.
(14) Tey, S.-K., Dotti, G., Rooney, C. M., Heslop, H. E., and Brenner, M. K. (2007) Inducible caspase 9 suicide gene to improve the safety of allodepleted T cells after haploidentical stem cell transplantation. *Biol. Blood Marrow Transplant. 13*, 913–924.
(15) Thiesen, B., and Jordan, A. (2008) Clinical applications of magnetic nanoparticles for hyperthermia. *Int. J. Hyperthermia 24*, 467–474.
(16) Huang, X., El-Sayed, I. H., Qian, W., and El-Sayed, M. A. (2006) Cancer Cell Imaging and Photothermal Therapy in the Near-Infrared Region by Using Gold Nanorods. *J. Am. Chem. Soc. 128*, 2115–2120.

(17) Piraner, D. I., Farhadi, A., Davis, H. C., Wu, D., Maresca, D., Szablowski, J. O., and Shapiro, M. G. (2017) Going Deeper: Biomolecular Tools for Acoustic and Magnetic Imaging and Control of Cellular Function. *Biochemistry 56*, 5202–5209.
(18) Haar, G., and Coussios, C. (2007) High intensity focused ultrasound: Physical principles and devices. *Int. J. Hyperthermia 23*, 89–104.
(19) Guilhon, E., Voisin, P., Zwart, J. A. de, Quesson, B., Salomir, R., Maurange, C., Bouchaud, V., Smirnov, P., Verneuil, H. de, Vekris, A., Canioni, P., and Moonen, C. T. W. (2003) Spatial and temporal control of transgene expression in vivo using a heat-sensitive promoter and MRI-guided focused ultrasound. *J. Gene Med. 5*, 333–342.
(20) Deckers, R., Quesson, B., Arsaut, J., Eimer, S., Couillaud, F., and Moonen, C. T. W. (2009) Image-guided, noninvasive, spatiotemporal control of gene expression. *Proc. Natl. Acad. Sci. U. S. A. 106*, 1175–1180.
(21) Kruse, D. E., Mackanos, M. A., O\textquotesingleConnell-Rodwell, C. E., Contag, C. H., and Ferrara, K. W. (2008) Short-duration-focused ultrasound stimulation of Hsp70 expressionin vivo. *Phys. Med. Biol. 53*, 3641–3660.
(22) Piraner, D. I., Abedi, M. H., Moser, B. A., Lee-Gosselin, A., and Shapiro, M. G. (2017) Tunable thermal bioswitches for *in vivo* control of microbial therapeutics. *Nat. Chem. Bio. 13*, 75–80.
(23) Piraner, D. I., Wu, Y., and Shapiro, M. G. (2019) Modular Thermal Control of Protein Dimerization. *ACS Synth. Biol. 8*, 2256–2262.
(24) Hildebrandt, B., Wust, P., Ahlers, O., Dieing, A., Sreenivasa, G., Kerner, T., Felix, R., and Riess, H. (2002) The cellular and molecular basis of hyperthermia. *Crit. Rev. Oncol. Hemat. 43*, 33–56.
(25) Rome, C., Couillaud, F., and Moonen, C. T. W. (2005) Spatial and temporal control of expression of therapeutic genes using heat shock protein promoters. *Methods 35*, 188–198.
(26) Wada, K.-I., Taniguchi, A., and Okano, T. (2007) Highly sensitive detection of cytotoxicity using a modified HSP70B′ promoter. *Biotechnol. Bioeng. 97*, 871–876.
(27) Kay, R. J., Boissy, R. J., Russnak, R. H., and Candido, E. P. (1986) Efficient transcription of a Caenorhabditis elegans heat shock gene pair in mouse fibroblasts is dependent on multiple promoter elements which can function bidirectionally. *Mol. Cell. Biol. 6*, 3134–3143.
(28) Miller, I. C., Gamboa Castro, M., Maenza, J., Weis, J. P., and Kwong, G. A. (2018) Remote Control of Mammalian Cells with Heat-Triggered Gene Switches and Photothermal Pulse Trains. *ACS Synth. Biol. 7*, 1167–1173.
(29) Ferreira, J. P., Overton, K. W., and Wang, C. L. (2013) Tuning gene expression with synthetic upstream open reading frames. *Proc. Natl. Acad. Sci. U. S. A. 110*, 11284–11289.
(30) Yamaguchi, M., Ito, A., Okamoto, N., Kawabe, Y., and Kamihira, M. (2012) Heat-inducible transgene expression system incorporating a positive feedback loop of transcriptional amplification for hyperthermia-induced gene therapy. *J. Biosci. Bioeng. 114*, 460–465.
(31) Søndergaard, H., and Skak, K. (2009) IL-21: roles in immunopathology and cancer therapy. *Tissue Antigens 74*, 467–479.
(32) Singh, H., Figliola, M. J., Dawson, M. J., Huls, H., Olivares, S., Switzer, K., Mi, T., Maiti, S., Kebriaei, P., Lee, D. A., Champlin, R. E., and Cooper, L. J. N. (2011) Reprogramming CD19-Specific T Cells with IL-21 Signaling Can Improve Adoptive Immunotherapy of B-Lineage Malignancies. *Cancer Res. 71*, 3516–3527.
(33) Parrish-Novak, J., Dillon, S. R., Nelson, A., Hammond, A., Sprecher, C., Gross, J. A., Johnston, J., Madden, K., Xu, W., West, J., Schrader, S., Burkhead, S., Heipel, M., Brandt, C., Kuijper, J. L., Kramer, J., Conklin, D., Presnell, S. R., Berry, J., Shiota, F., Bort, S., Hambly, K., Mudri, S., Clegg, C., Moore, M., Grant, F. J., Lofton-Day, C., Gilbert, T., Raymond, F., Ching, A., Yao, L., Smith, D., Webster, P., Whitmore, T., Maurer, M., Kaushansky, K., Holly, R. D., and Foster, D. (2000) Interleukin 21 and its receptor are involved in NK cell expansion and regulation of lymphocyte function. *Nature 408*, 57–63.
(34) Xu, Y., Hyun, Y.-M., Lim, K., Lee, H., Cummings, R. J., Gerber, S. A., Bae, S., Cho, T. Y., Lord, E. M., and Kim, M. (2014) Optogenetic control of chemokine receptor signal and T-cell migration. *Proc. Natl. Acad. Sci. U.S.A. 111*, 6371–6376.
(35) McDannold, N. J., King, R. L., Jolesz, F. A., and Hynynen, K. H. (2000) Usefulness of MR Imaging-Derived Thermometry and Dosimetry in Determining the Threshold for Tissue Damage Induced by Thermal Surgery in Rabbits. *Radiology 216*, 517–523.
(36) McDannold, N., Vykhodtseva, N., Jolesz, F. A., & Hynynen, K. (2004) MRI investigation of the threshold for thermally induced blood-brain barrier disruption and brain tissue damage in the rabbit brain. *Magn. Reson. Med. 51*, 913–923.
(37) Kregel, K. C. (2002) Invited Review: Heat shock proteins: modifying factors in physiological stress responses and acquired thermotolerance. *J. Appl. Physiol. 92*, 2177–2186.

(38) Morimoto, R. I. (1998) Regulation of the heat shock transcriptional response: cross talk between a family of heat shock factors, molecular chaperones, and negative regulators. *Genes Dev. 12*, 3788–3796.

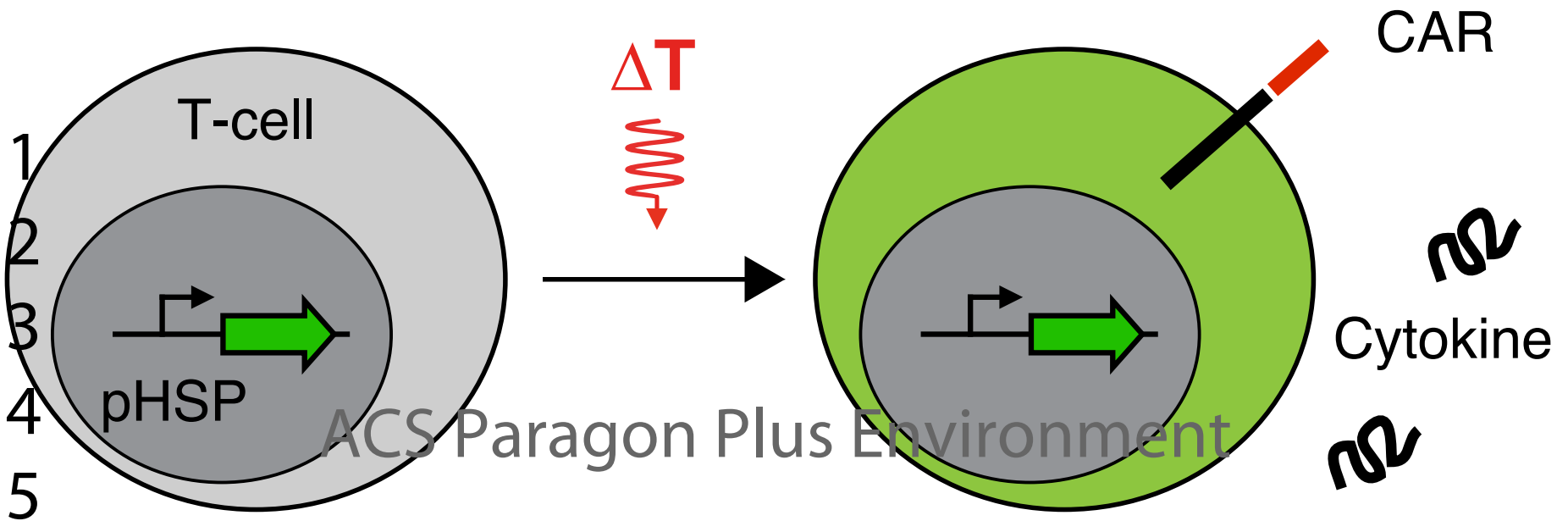

a

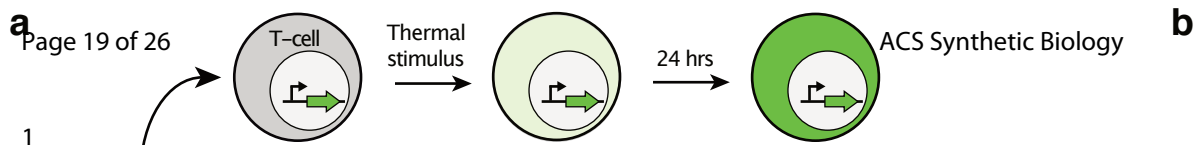

HSP				
HSPB	(Human)			
HSPB'1	(Human)	HSPA/A	(Human)	
HSPB'2	(Human)	HSPA/B	(Human)	
HSPB'3	(Human)	HSPm1	(Mouse)	
SynHSPB'1	(Human)	HSPm2	(Mouse)	
SynHSPB'2	(Human)	HSPm3	(Mouse)	
SynHSPB'3	(Human)	HSP16F	(C. elegans)	

Analyze cells:

- Select live BFP^{+} cells
- Quantify GFP fluorescence

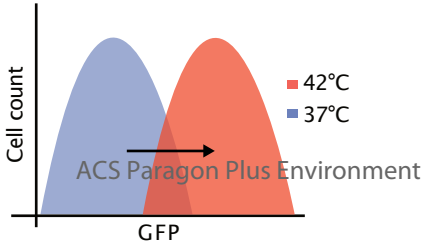

b

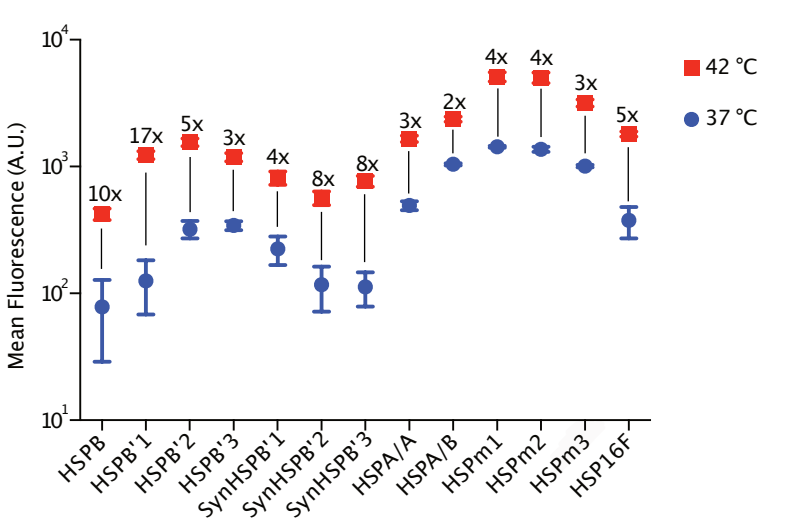

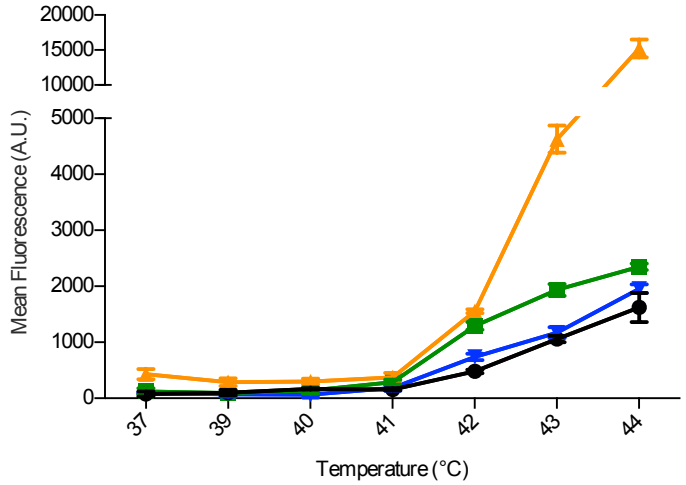
a
Mean Fluorescence (A.U.)
20000
15000
10000
5000
4000
3000
2000
1000
0
37
39
40
41
42
43
44
Temperature (°C)
SynHSPB'3
HSP16F
HSPB'1
HSPB

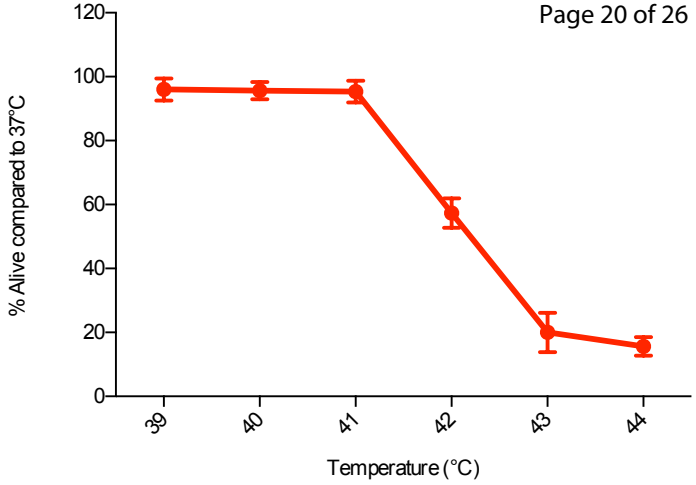
b
% Alive compared to 37°C
120
100
80
60
40
20
0
39
40
41
42
43
44
Temperature (°C)

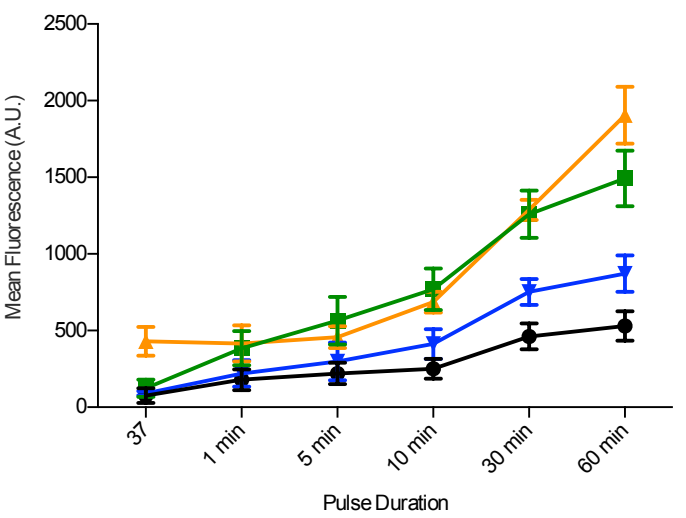
c
Mean Fluorescence (A.U.)
2500
2000
1500
1000
500
0
37
1 min
5 min
10 min
30 min
60 min
Pulse Duration
SynHSPB'3
HSP16F
HSPB'1
HSPB

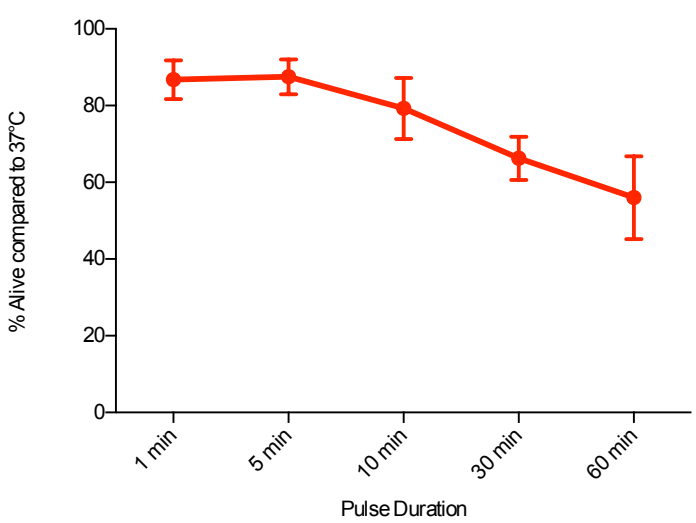
d
% Alive compared to 37°C
100
80
60
40
20
0
1 min
5 min
10 min
30 min
60 min
Pulse Duration

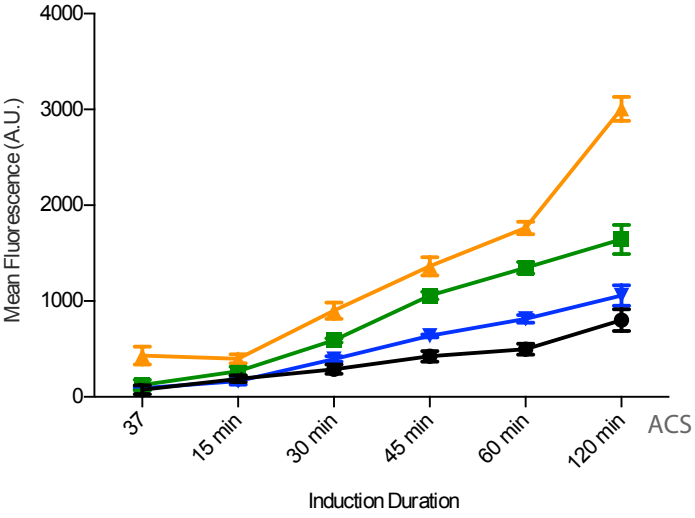
e
Mean Fluorescence (A.U.)
4000
3000
2000
1000
0
37
15 min
30 min
45 min
60 min
120 min
Induction Duration
SynHSPB'3
HSP16F
HSPB'1
HSPB

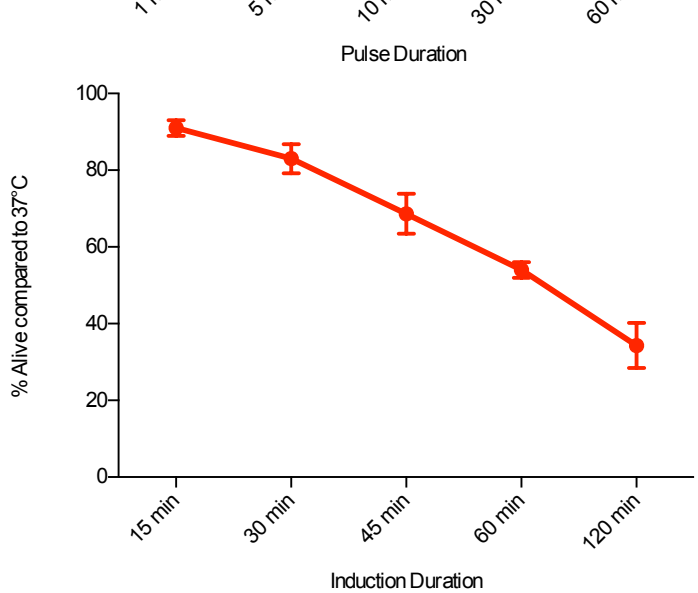
f
% Alive compared to 37°C
100
80
60
40
20
0
15 min
30 min
45 min
60 min
120 min
Induction Duration

a

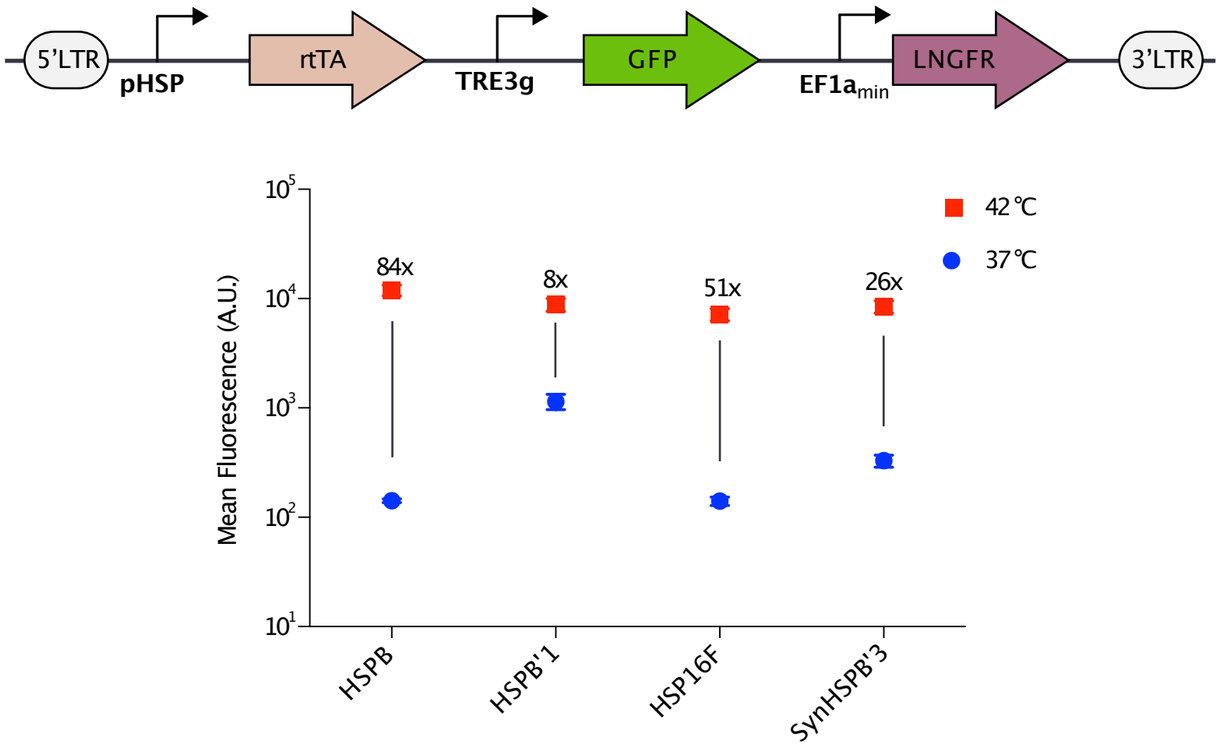
5'LTR
pHSP
rtTA
TRE3g
GFP
EF1a$_{min}$
LNGFR
3'LTR
Mean Fluorescence (A.U.)
10^5
10^4
10^3
10^2
10^1
84x
8x
51x
26x
42 °C
37 °C
HSPB
HSPB'1
HSP16F
SynHSPB'3

b

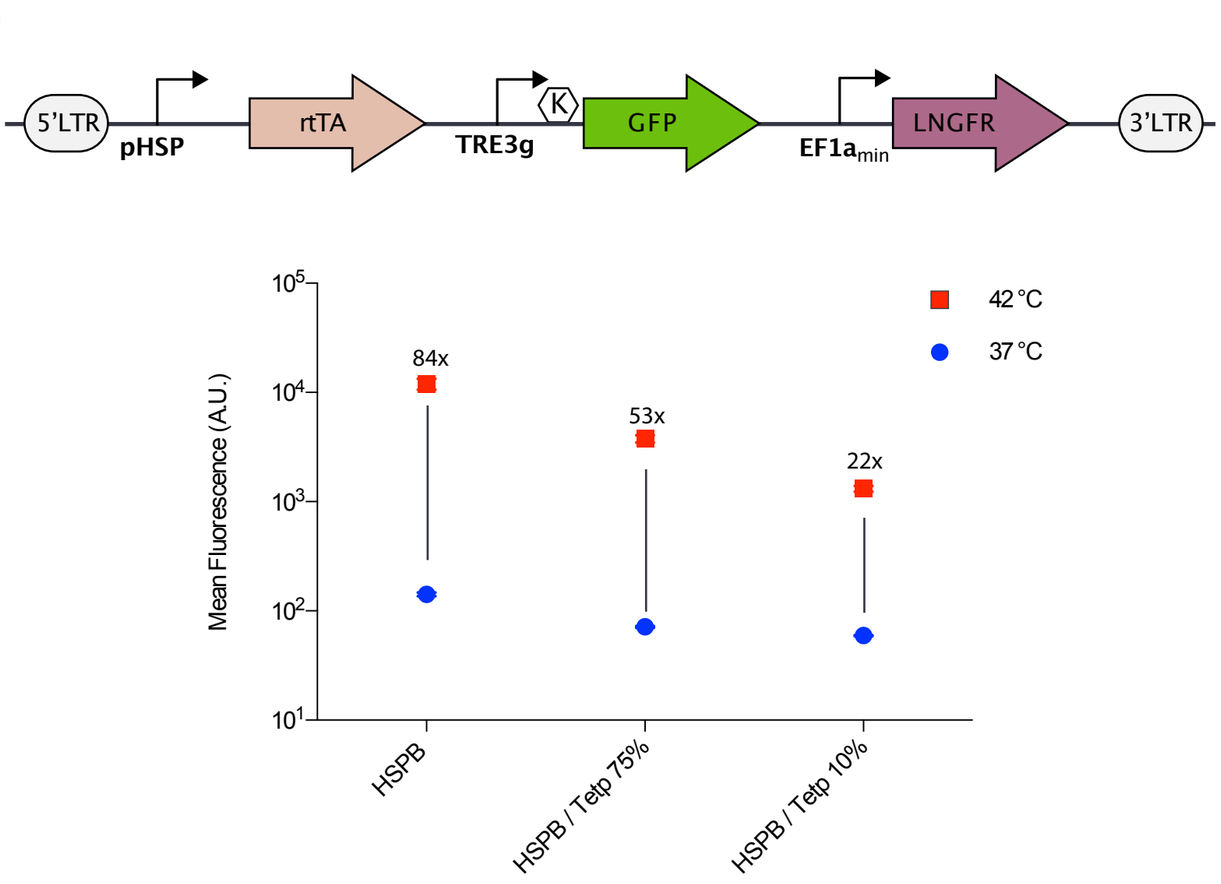
5'LTR
pHSP
rtTA
TRE3g
K
GFP
EF1a$_{min}$
LNGFR
3'LTR
Mean Fluorescence (A.U.)
10^5
10^4
10^3
10^2
10^1
84x
53x
22x
42 °C
37 °C
HSPB
HSPB / Tetp 75%
HSPB / Tetp 10%

c

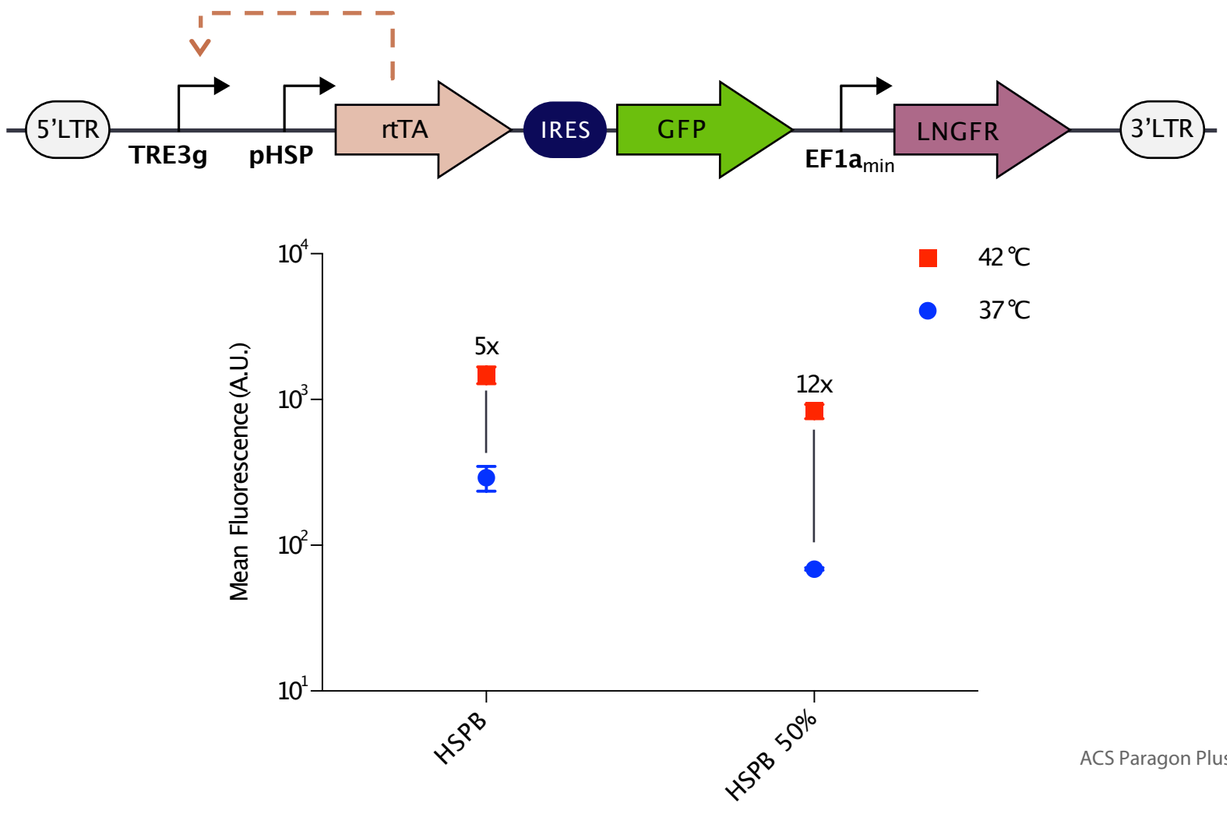
5'LTR
TRE3g
pHSP
rtTA
IRES
GFP
EF1a$_{min}$
LNGFR
3'LTR
Mean Fluorescence (A.U.)
10^4
10^3
10^2
10^1
5x
12x
42 °C
37 °C
HSPB
HSPB 50%

d

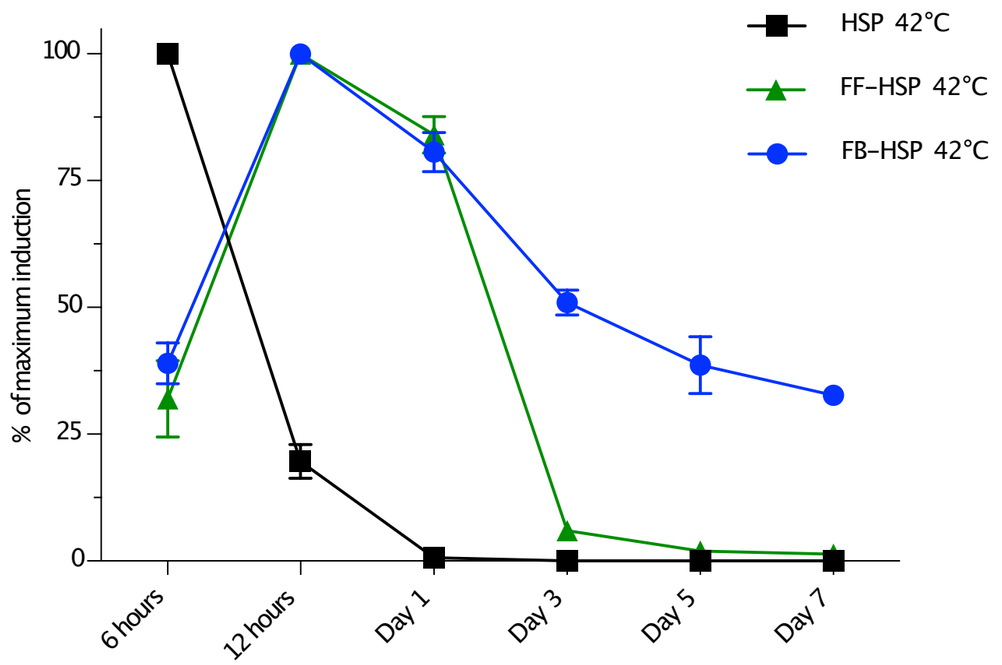
% of maximum induction
100
75
50
25
0
HSP 42°C
FF–HSP 42°C
FB–HSP 42°C
6 hours
12 hours
Day 1
Day 3
Day 5
Day 7

e

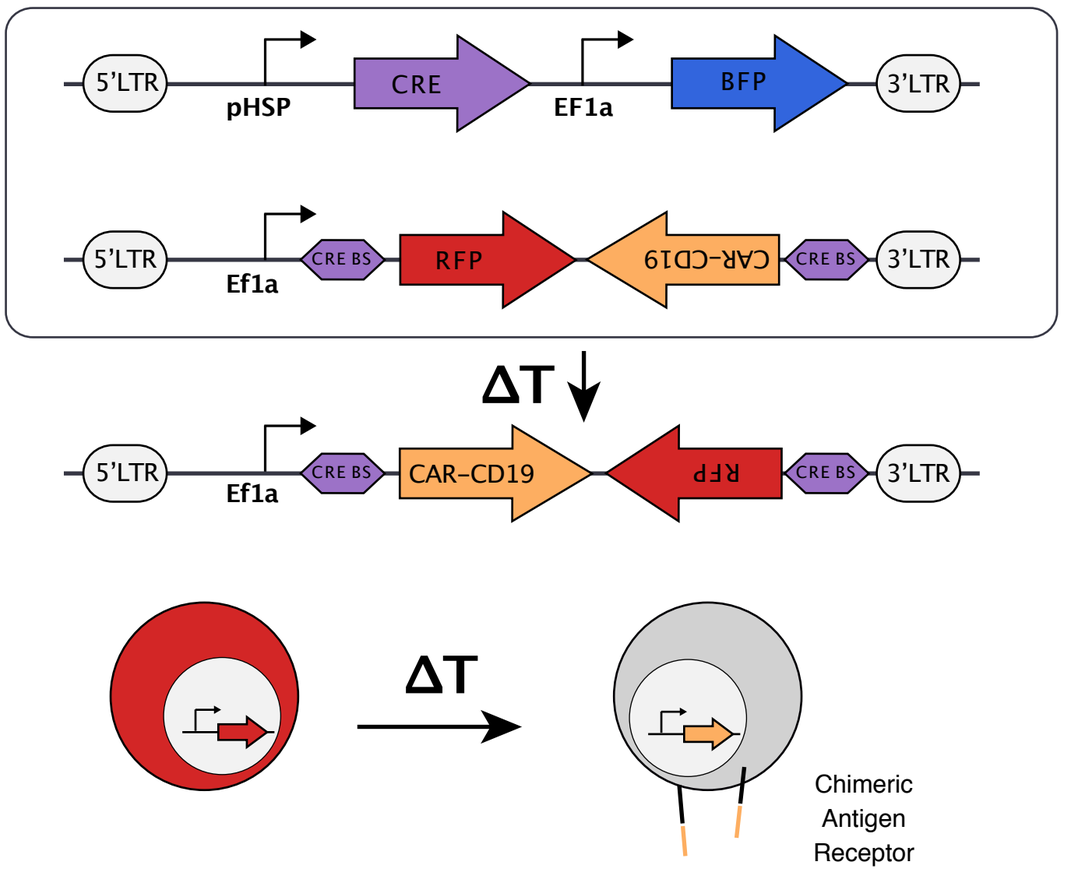
5'LTR
pHSP
CRE
EF1a
BFP
3'LTR
5'LTR
Ef1a
CRE BS
RFP
CAR-CD19
CRE BS
3'LTR
ΔT
5'LTR
Ef1a
CRE BS
CAR-CD19
RFP
CRE BS
3'LTR
ΔT
Chimeric
Antigen
Receptor

f

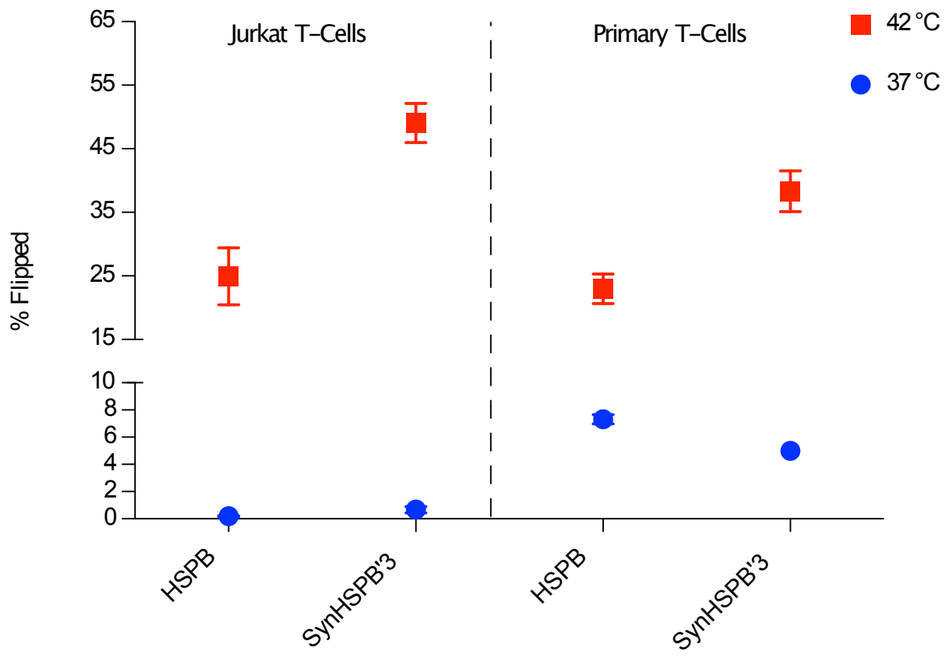
% Flipped
65
55
45
35
25
15
10
8
6
4
2
0
Jurkat T–Cells
Primary T–Cells
42 °C
37 °C
HSPB
SynHSPB'3
HSPB
SynHSPB'3

6et

a

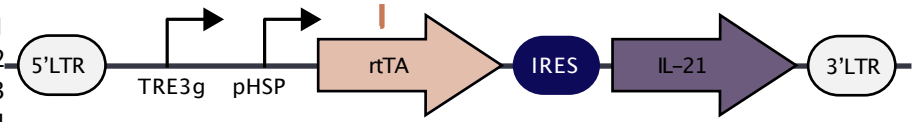

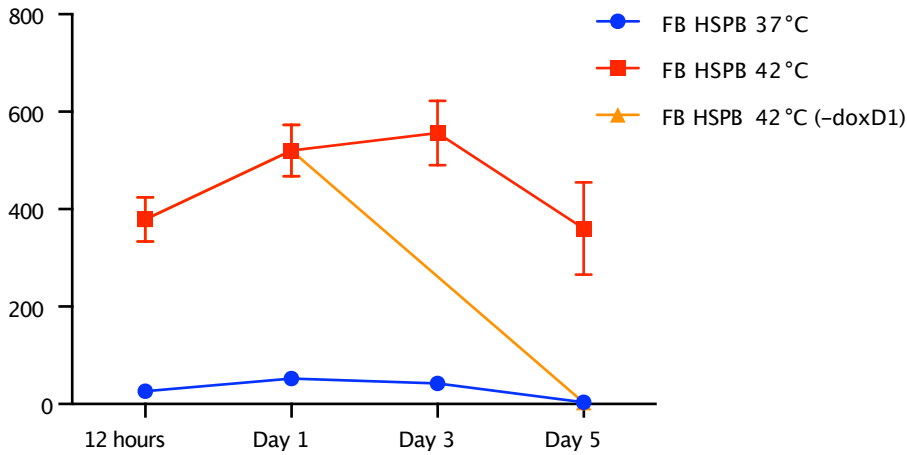

b

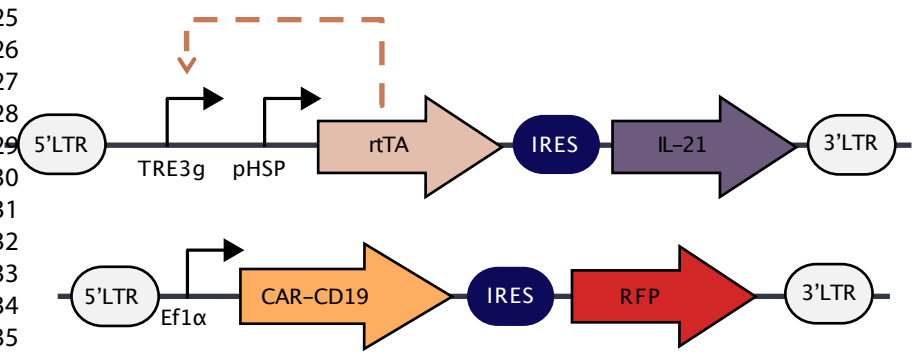

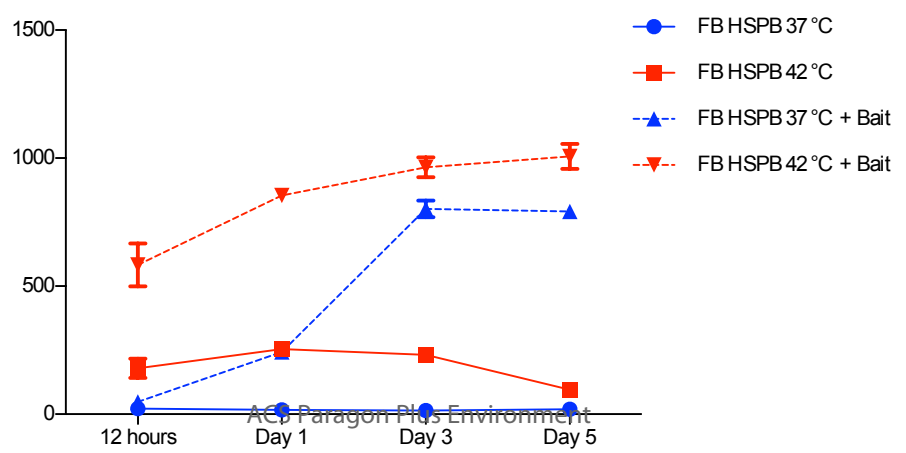

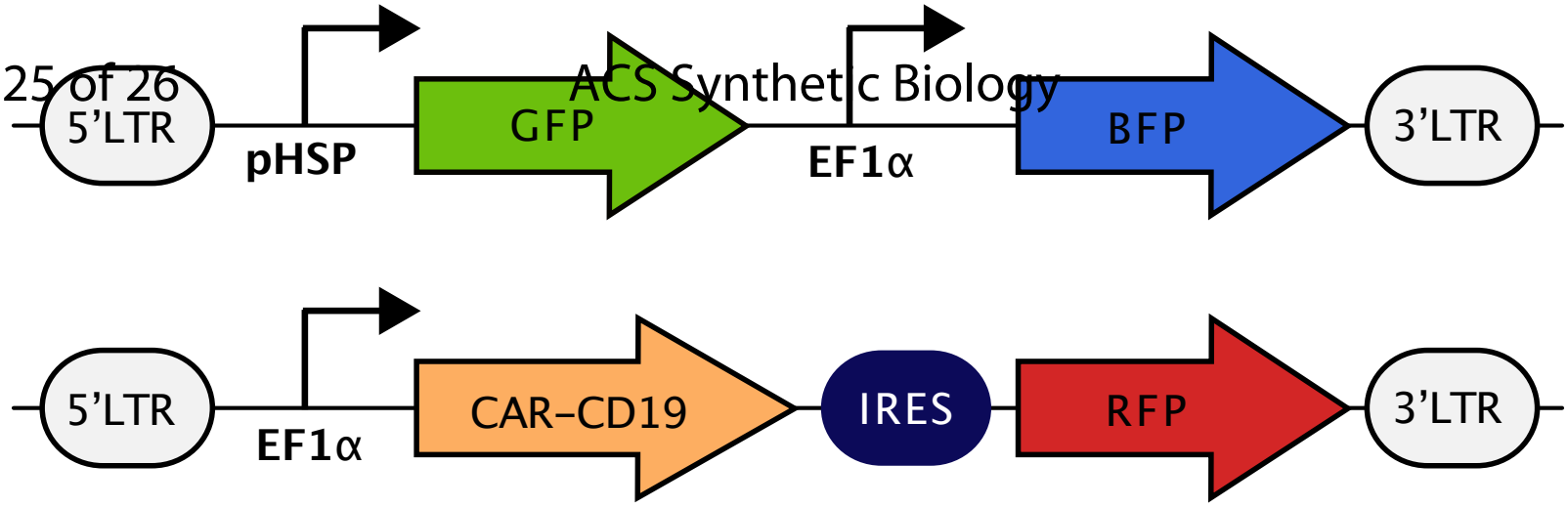
a
5'LTR
pHSP
GFP
EF1α
BFP
3'LTR
5'LTR
EF1α
CAR-CD19
IRES
RFP
3'LTR

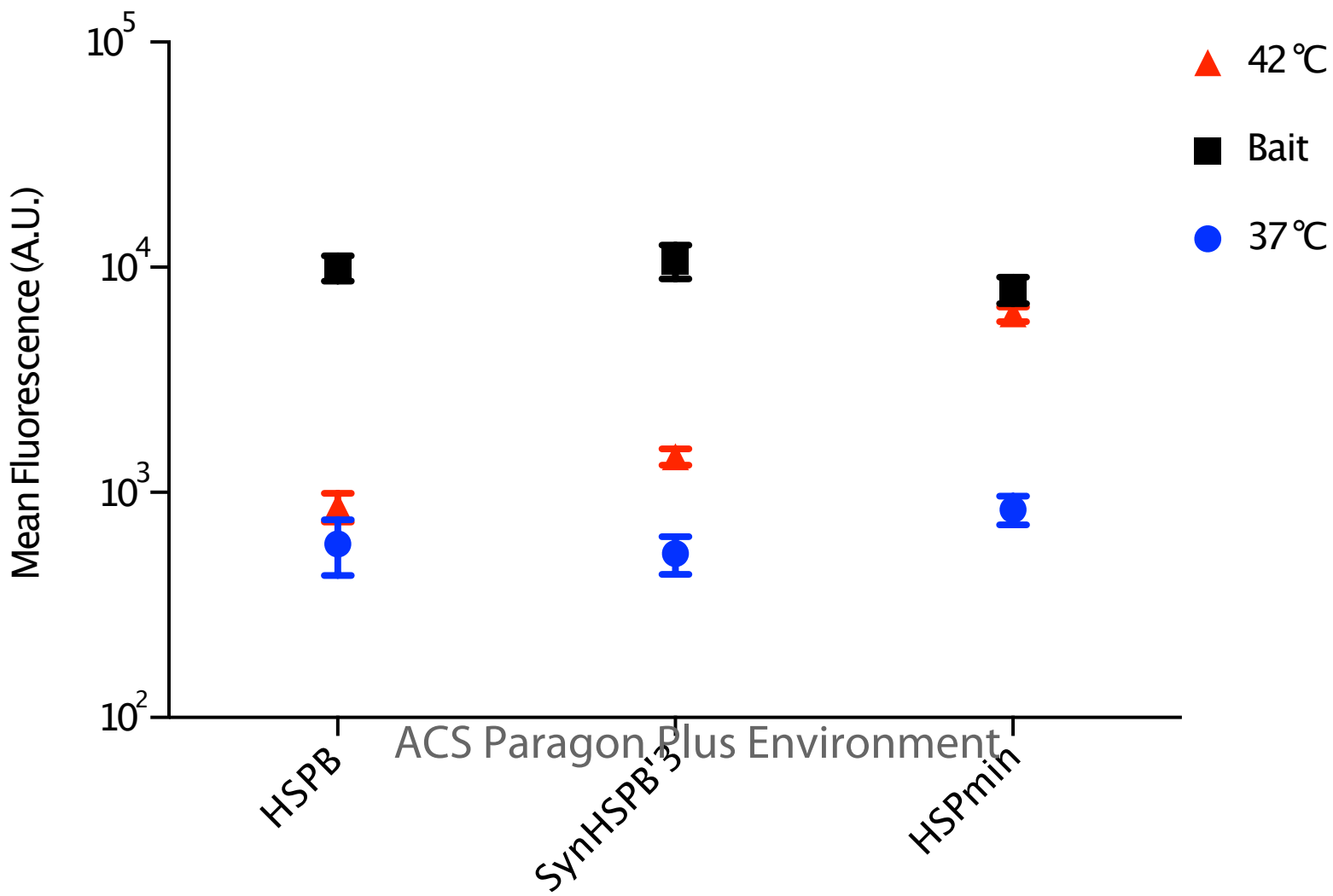
b
Mean Fluorescence (A.U.)
10^5
10^4
10^3
10^2
42 ℃
Bait
37 ℃
HSPB
SynHSPB'3
HSPmin
ACS Paragon Plus Environment